FUEL PIN BUNDLE EXPERIMENTAL CHARACTERIZATION IN HLM LARGE POOL SYSTEM

Martelli D., Barone G., Forgione N., Angelucci M.
Department of Civil and Industrial Engineering,
University of Pisa
Largo Lucio Lazzarino 2, 56122 Pisa, Italy
daniele.martelli@ing.unipi.it; nicola.forgione@ing.unipi.it; gianluca.barone@for.unipi.it;
morena.angelucci@for.unipi.it

Tarantino M., Di Piazza I., Agostini P.
Italian National Agency for New Technologies, Energy
and Sustainable Economic Development, Brasimone R.C.
ENEA UTIS-TCI, C.R. Brasimone, 40032 Camugnano (Bo), Italy
mariano.tarantino@enea.it; ivan.dipiazza@enea.it; pietro.agostini@enea.it

ABSTRACT

In the context of GEN IV innovative nuclear reactor design, Lead Fast Reactor (LFR) represents a promising alternative to Sodium Fast Reactor (SFR). European Research Community is promoting R&D programs to guide the design of Pilot Plant for the advancement of lead fast reactor technology. For this purpose, ENEA Brasimone R.C. is conducting several thermal-hydraulic experimental campaigns aiming at supporting the design of the Multipurpose Hybrid Research Reactor for High-tech Application (MYRRHA).
ENEA is involved in fuel pin & assembly thermal-hydraulic investigations through experimental activities on the NACIE loop type and CIRCE pool type facilities. The aim of this work, performed in the frame of the partnership ENEA-Pisa University, is the investigation of heat transfer phenomena in fuel rod bundles in a pool type configuration.
The obtained experimental data represent the first data published for LBE coolant in a pool type configuration. The experimental campaign is conducted on the CIRCE-ICE (Circulation Eutectic in the Integral Circulation Experiment configuration) facility, filled with 70 tons of molten LBE. A series of experiments performed in natural and forced circulation regimes are carried out and obtained data are post-processed obtaining a Nusselt characterization in the central subchannel of the bundle as function of the Peclet number in a Peclet range of 500-3000.
Experimentally determined values, are then compared with correlations available in the HLM literature (obtained using NaK or Hg as working fluid), showing a linear trend as the Pe increases, in agreement with the proposed correlations, showing a general tendency to lie below them. In particular, the Nu numbers obtained from the experimental data are about 25% lower than data predicted from correlations by less than 25%. Moreover, the paper reports a preliminary analysis and discussion of such results, also in comparison with CFD calculations performed by CFX code.

KEYWORDS
CIRCE, HLM, MYRRHA, LMFR, NUSSELT, FUEL PIN

1. INTRODUCTION

Within the Generation IV Nuclear reactor international task force (GEN IV International Forum, 2014 [1]), the European Commission (European Sustainable Nuclear Industrial Initiatives ESNII) is supporting three GEN IV fast reactor projects (Sodium, Lead and Gas cooled fast reactors) as part of the EU's plan to promote low-carbon energy technologies (SNE-TP, 2013, [2]). The sodium-cooled fast neutron reactor technology is actually considered the reference solution primarily for Europe's prior experience in sodium technology. Nevertheless, a Lead-cooled fast reactor is the most promising alternative technology for fast reactors. Since lead interaction with water or air is less critical compared with the interaction between sodium and water or air, the intermediate loop typical of SFR can be eliminated reducing the complexity of the plant and its cost and increasing its safety. Moreover, the LFR showed advantages over the SFR regarding behaviour in severe accidents like ULOF, ULOHS and TLOP (Tuček et al., 2006, [3]). Another attractive advantage of the LFR is the low amount of potential (non-nuclear) energy stored in the reactors' primary circuit (twenty times lower than in a water-cooled reactor and ten times lower than in sodium coolant respectively, Toshinsky et al., 2013, [4]). Potential energy is an inherent coolant property and cannot be overtaken by engineering solutions. As already mentioned, lead coolant is chemically inert with air and water hence no chemical energy is stored in the coolant, moreover thanks to the high boiling temperature (about 2016±10 K for lead, see Sobolev, 2007, [5]) the pressure can be maintained at atmospheric value (no coolant compression energy stored). Currently, ENEA has implemented large competencies and capabilities in the field of HLM thermal-hydraulics, coolant technology, materials for high temperature applications, corrosion and material protection, heat transfer and removal, component development and testing, remote maintenance, procedure definition and coolant handling. In this frame, the Integral Circulation Experiment (ICE) test section was installed into the CIRCE pool facility, and suitable experiments have been carried out aiming to deeply investigate heat transfer phenomena and pool thermal-hydraulic behaviour of a HLM cooled pool reactor. An electrical Fuel Pin Simulator (FPS) was installed in the CIRCE pool, conceived with a thermal power of about 1 MW and a linear power up to 25 kW/m. Along its active length four different sections were deeply instrumented to monitor the heat transfer coefficient along the bundle as well as the cladding temperature in different ranks of sub-channels. A full characterization of the FPS was experimentally achieved in the natural and forced circulation regime. The Nusselt number was calculated as a function of the Peclet number and the experimental results were compared to the Nusselt number computed from correlations available in the literature and calculated by CFD numerical simulations.

2. ICE FUEL PIN SIMULATOR

The ICE FPS represents the Heat Source (HS) of the system; it consists of an electrical bundle made up of 37 pins arranged in a hexagonal wrapped lattice (see Figure 1) with a pitch to diameter ratio of 1.8. The main parameters are summarized in Table 1. The FPS has been conceived with a thermal power of about 1 MW and a linear power up to 25kW/m, relevant values for MYRRHA reactor and Liquid Metal Fast Reactor (LMFR) in general. The relative position between the pin bundle and the wrapper is assured by three appropriate spacer grids placed along the axis of the component and fixed to the wrapper. The upper and lower spacer grids were placed at the interface between the active and non-active length of the electrical pins to enclose the mixing zones. The middle spacer grid was placed in the middle section of the bundle active length. Figure 1, shows the FPS cross section.

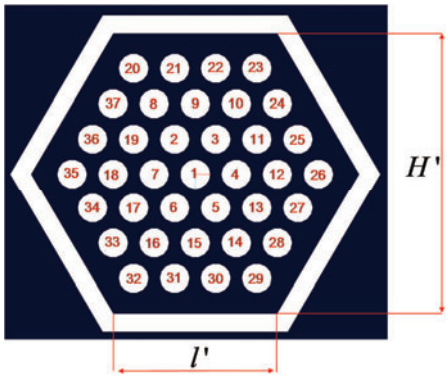

Figure 1: HS cross section (l' = 55.4 mm, H' = 96 mm)

Table 1: Main parameters

Parameter	Symbol	Value
Number of Pins	n	37
Pin outer Parameter	Φ [mm]	8.2
Power of a pin	[kW]	25
Pin wall heat flux	[MW/m^2]	1
Pitch-to-diameter ratio	p/d	1.8
Pin clad material	-	AISI 316L
Active Length	L [mm]	1000
Edge length	l' [mm]	55.4
Apothem	$H'/2$ [mm]	48

In order to investigate the heat transfer in a HLM-cooled rod bundle, the FPS was instrumented with several *N* type thermocouples having a diameter of 0.5 mm with an isolated hot junction and an accuracy of ±0.1°C. Regarding the positioning of the thermocouples along the FPS active zone, four different sections were monitored (Figure 2):

- Section 1: 20 mm upstream of the middle spacer grid. In this section three different sub-channels were instrumented (see Figure 3 (*a*)). In each sub-channel both pin clad and LBE bulk temperatures were measured (TC-FPS-01 ... 09).
- Section 2: on the matching surface between the middle spacer grid and the fuel pins (see Figure 3 (*b*)). In this section the same sub-channels were identified as in the section 1, aiming at the hot spot factor evaluation due to the installation of the spacer grid itself. In this case, only the pin clad temperature was monitored by TCs (TC-FPS-10 ... 14).
- Section 3: 60 mm upstream of the upper spacer grid. In this section, the same sub-channels were identified as in sections 1 and 2 for temperature measurements in the upper part of the bundle (see Figure 3 (*a*)). In each sub-channel both pin clad and LBE bulk temperatures were measured by TCs (TC-FPS-16 ... 24).
- Section 4: 60 mm downstream of the lower spacer grid (see Figure 3 (*b*)). In this section, the LBE centre channel temperature was measured in each sub-channel (TC-FPS-28 ... 30).

Thermocouples mounted on the pin wall, are kept in place by a thin metal sheet welded on the pin clad, while thermocouple in the middle of the channel are guided and held in position through a small steel tube as shown in Figure 4. Furthermore, an additional correction for the wall temperature is required to take into account the exact position of the thermocouple fixed to the pin external wall with an AISI 304 sheet. Considering the thermal conduction phenomena, the applied correction is given by:

$$T_{W,corr} = T_{W,\exp} + \frac{\dot{Q}}{N\pi D_{pin} L_{heat}} \cdot \frac{D_{TC}/2}{k_{AISI\,304}} \tag{1}$$

where D_{TC} is the diameter of the thermocouple and L_{heat} is the active pin length and $\dot{Q}$ is the thermal power supplied to the FPS.

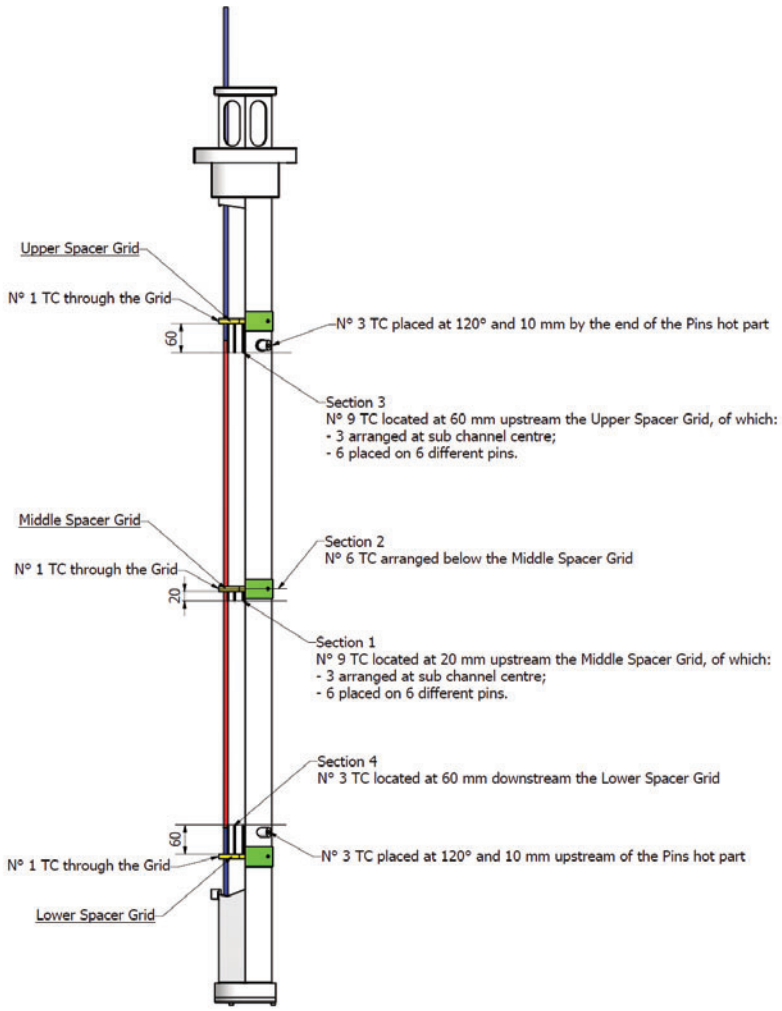

Figure 2: FPS measurement sections

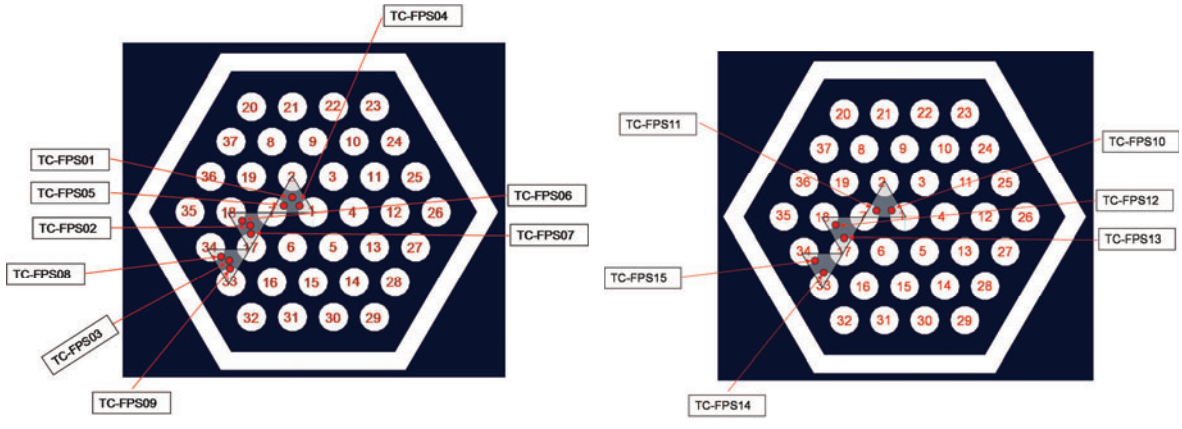

(*a*) (*b*)

Figure 3: Section 1 (*a*) and Section 2 (*b*) sub channel instrumentation

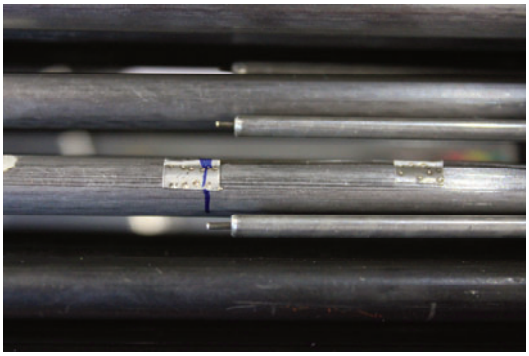

Figure 4: Details of thermocouples inside the FPS structure

3. EXPERIMENTAL AND NUMERICAL RESULTS

This experimental campaign under investigation was focused on the characterization of heat transfer in a fuel bundle in natural (*NC*) and forced (*FC*) circulation conditions. In particular, *FC* tests were carried out imposing a temperature difference through the FPS of about 80°C and the electrical power supplied to the FPS was calculated by the energy balance imposing the desired LBE mass flow rate through the FPS. Sub-channel temperatures were investigated at different Peclet numbers, by changing the LBE mass flow rate in the range of 40-70 kg/s (in steps of about 5 kg/s). Concerning *NC* tests, the power into the FPS, was changed from 100 kW to 600 kW in steps of 100 kW allowing to investigate LBE flow rate through the test section in the range between 12-25 kg/s. For each step, steady state temperature conditions in the FPS were reached and maintained at least for 15 min. Nusselt number was evaluated in the central sub-channel both in Section 1 and in Section 3. All data reported in the paper refers to the central subchannel of the FPS and a reasonable approximation is to consider the central subchannel as being representative of an infinite lattice.
In Table 2, the adopted boundary conditions are summarized. In particular, the imposed LBE mass flow rate, argon flow rate to reach the desired LBE mass flow rate and FPS electrical power to obtain the desired difference in temperature between the FPS inlet and outlet section are reported.

Table 2: Performed experimental tests

Name	LBE Mass flow rate [kg/s]	Argon Mass flow rate [Nl/s]	FPS Electrical Power [kW]
1-*FC*	70	5.00	800
2-*FC*	65	4.40	760
3-*FC*	60	3.00	700
4-*FC*	55	2.40	640
5-*FC*	50	1.60	580
6-*FC*	45	1.45	525
7-*FC*	40	1.41	465
1-*NC*	25	600	165
2-*NC*	23	500	151
3-*NC*	21	400	133
4-*NC*	19	300	109
5-*NC*	14	200	102
6-*NC*	12	100	58

Sources of error in the experimental measurements are considered and the effect of the uncertainty for each measured variable on the calculated results is investigated (Lichten, 1999 [6] and Moffat, 1988 [7]). Moreover, in order to obtain a standard deviation representative of the dispersion and neglecting effects

due to an imperfect stationarity of acquired experimental variables, a linear regression for each gained thermocouple signal was evaluated and subtracted from the original one. In particular, linear regression was computed using the Ordinary Least Squares method (OLS). The statistical standard deviation was finally calculated using the modified data. Figure 5 (*a*), shows temperature data in the centre of the channel and its linear regression for Test 1-*FC*; after 15 mins the temperature decreases by about 1°C. Figure 5 (*b*) shows the modified temperature values obtained reducing the modified source signal by its linear regression.

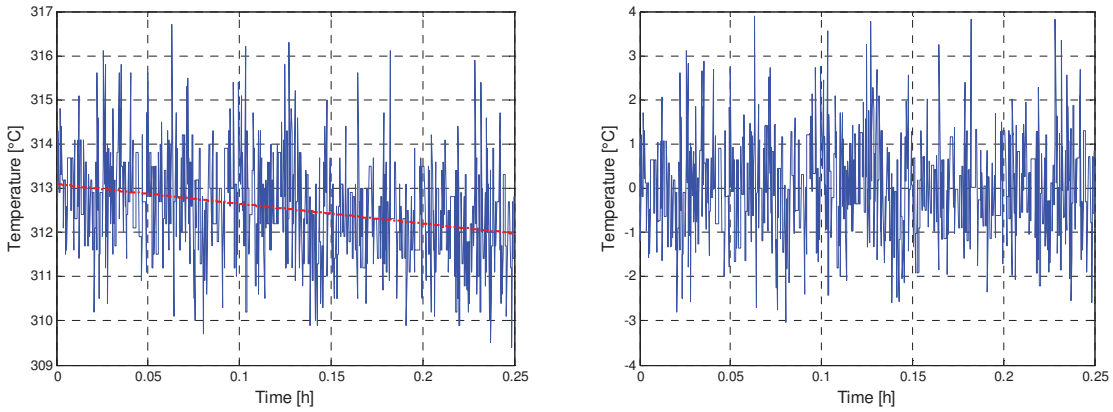

(*a*) (*b*)

Figure 5: Test 1-FC, temperature in the centre of the channel (a) and modified signal for statistical calculations (b)

In the calculation of the Nu number, stationary conditions for the temperature difference between the wall and the bulk are confirmed. Regarding the coolant thermo-physical properties, all the empirical correlations used in this work are in agreement with the correlations for Lead-bismuth Eutectic available in the Handbook on Lead-bismuth Eutectic alloy, 2007 [8] and their own accuracy is considered. The Nusselt number was calculated in Section 1 and Section 3 respectively for the central sub-channel according to the following formula:

$$Nu = \frac{HTC \cdot d_{eq}}{k} \tag{2}$$

where d_{eq} is the equivalent diameter for a triangular array interior channel and for an infinite lattice. The heat transfer coefficient is calculated by the Newton relationship HTC=$q''/(T_c-T_b)$, where q'' is the heat flux obtained from an energy balance in order to account heat losses from the FPS wrapper to the surrounding LBE in the pool, T_c and T_b are the clad and the coolant bulk temperatures respectively. The bulk temperature on the middle and upper sections is obtained considering a linear trend between the average temperature values at the entrance and at the exit of FPS active length.

In tables 3 and 4, Nu values computed for all the performed experimental tests are reported together with Pe and Re numbers. All these non-dimensional numbers are secondary variables, hence propagation of errors are taken into account and reported as well.

Table 3: Obtained results at Section 1 and their uncertainties

Name	Re	$\langle\sigma_X\rangle$	$\left\langle\frac{\sigma_X}{X}\right\rangle$	Pe	$\langle\sigma_X\rangle$	$\left\langle\frac{\sigma_X}{X}\right\rangle$	Nu	$\langle\sigma_X\rangle$	$\left\langle\frac{\sigma_X}{X}\right\rangle$
1-FC	$1.4\ 10^5$	$7.8\ 10^3$	5.6%	2933	263	9%	26.3	2.6	10.0%
2-FC	$1.3\ 10^5$	$7.4\ 10^3$	5.7%	2772	249	9%	25.8	2.6	10.1%
3-FC	$1.2\ 10^5$	$7.0\ 10^3$	6.0%	2572	237	9%	26.0	2.7	10.4%
4-FC	$1.1\ 10^5$	$6.5\ 10^3$	6.0%	2365	218	9%	23.9	2.5	10.5%
5-FC	$9.5\ 10^4$	$6.8\ 10^3$	7.1%	2122	212	10%	23.8	2.9	12.3%
6-FC	$8.3\ 10^4$	$7.5\ 10^3$	9.0%	1896	217	11%	23.0	3.5	15.3%
7-FC	$7.6\ 10^4$	$7.4\ 10^3$	9.7%	1776	213	12%	23.2	3.8	16.6%
1-NC	$5.\ 710^4$	$3.1\ 10^3$	5.5%	984	88	9%	20.3	2.1	10.1%
2-NC	$5.2\ 10^4$	$3.0\ 10^3$	5.7%	903	82	9%	20.0	2.1	10.3%
3-NC	$5.0\ 10^4$	$2.8\ 10^3$	5.6%	796	71	9%	17.8	1.8	10.2%
4-NC	$4.5\ 10^4$	$2.5\ 10^3$	5.6%	738	66	9%	17.7	1.7	9.9%
5-NC	$3.0\ 10^4$	$1.7\ 10^3$	5.7%	579	52	9%	18.8	3.2	16.9%
6-NC	$2.5\ 10^4$	$1.4\ 10^3$	5.8%	542	49	9%	17.2	2.3	13.2%

Table 4: Obtained results at Section 3 and their uncertainties

Name	Re	$\langle\sigma_X\rangle$	$\left\langle\frac{\sigma_X}{X}\right\rangle$	Pe	$\langle\sigma_X\rangle$	$\left\langle\frac{\sigma_X}{X}\right\rangle$	Nu	$\langle\sigma_X\rangle$	$\left\langle\frac{\sigma_X}{X}\right\rangle$
1-FC	$1.5\ 10^5$	$8.4\ 10^3$	5.6%	2812	252	9%	24.5	2.3	9.3%
2-FC	$1.4\ 10^5$	$8.0\ 10^3$	5.7%	2657	239	9%	23.6	2.2	9.4%
3-FC	$1.3\ 10^5$	$7.6\ 10^3$	6.0%	2462	227	9%	23.0	2.3	9.8%
4-FC	$1.2\ 10^5$	$7.0\ 10^3$	6.0%	2266	209	9%	21.2	2.1	9.9%
5-FC	$1.0\ 10^5$	$7.4\ 10^3$	7.1%	2031	203	10%	21.1	2.4	11.4%
6-FC	$9.0\ 10^4$	$8.1\ 10^3$	9.0%	1811	207	11%	20.7	3.0	14.4%
7-FC	$8.2\ 10^4$	$8.0\ 10^3$	9.7%	1698	204	12%	20.6	3.3	16.0%
1-NC	$6.4\ 10^4$	$3.6\ 10^3$	5.5%	903	80	9%	18.0	1.8	9.8%
2-NC	$5.9\ 10^4$	$3.4\ 10^3$	5.7%	835	76	9%	17.4	1.7	9.9%
3-NC	$5.5\ 10^4$	$3.1\ 10^3$	5.6%	745	67	9%	15.5	1.4	9.3%
4-NC	$4.8\ 10^4$	$2.7\ 10^3$	5.6%	698	63	9%	14.3	1.4	9.7%
5-NC	$3.2\ 10^4$	$1.9\ 10^3$	5.7%	548	50	9%	13.7	1.9	13.9%
6-NC	$2.6\ 10^4$	$1.5\ 10^3$	5.8%	524	48	9%	12.5	1.6	12.9%

A CFD model of the ICE bundle was developed and pre-test computations were carried out to compare experimental results with computational results and to have a detailed overview of the local phenomena occurring in the wrapped bundle and in the spacer grid region.

The computational grid was designed to be accurate for the higher Reynolds number according to the ICE experiments (with an average axial velocity w_0~1 m/s, the sub-channel Reynolds number based on the hydraulic diameter is Re_{sc}~$1.31\cdot10^5$). The spatial resolution chosen implies y^+~1 in the first node close to the wall in the whole domain; therefore, the mechanical viscous sublayer is described by 8-10 grid points. The total number of cells of the model is about $1.24\cdot10^7$. The resolution of the thermal boundary layer is automatically guaranteed, being the Prandtl number of the fluid Pr~0.019. The model is fully structured, includes the conjugate heat transfer in the three spacer grids and the entry non-active zone. The grid-independence was verified as well.

The *SST* (Shear Stress Transport) k-ω model by Menter was extensively used in this work. A second order closure *RSM*-ε model (Reynolds Stress Model) was also used; this latter model has separate equations for the various Reynolds Stresses and thus it allows capturing the turbulence transport anisotropy to be captured.

The geometrical domain reproduced an angle of 60° of the 37-pin bundle and periodic boundaries conditions were assumed (Figure 6).

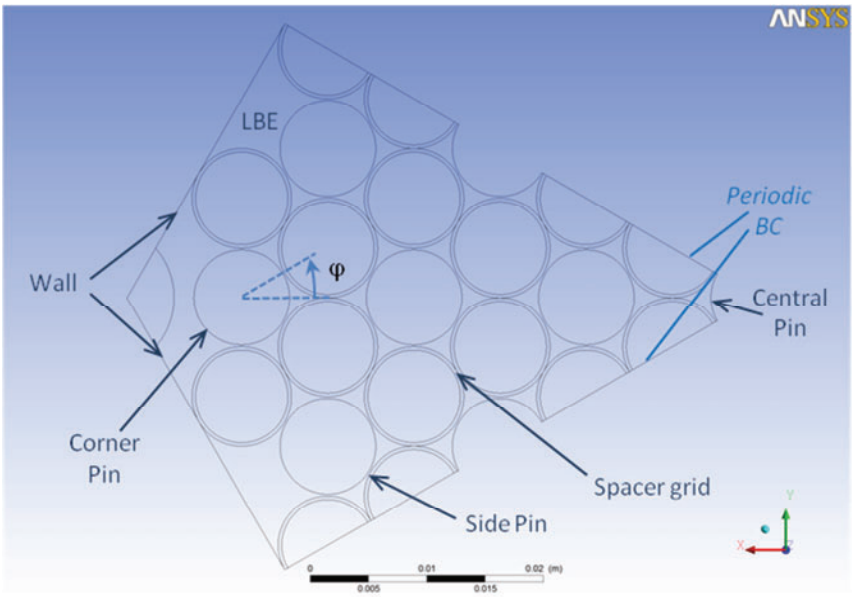

Figure 6: Thirty-seven Pin bundle computational domain with boundary conditions

A 3D detailed view of the middle spacer grid region is shown in Figure 7. A non-active entry region of 350 mm was reproduced in order to allow the flow to be hydrodynamically fully developed at the beginning of the active region. The length of the active region is 1 m. Downstream of the upper grid a non-active region of 350 mm was designed as well.

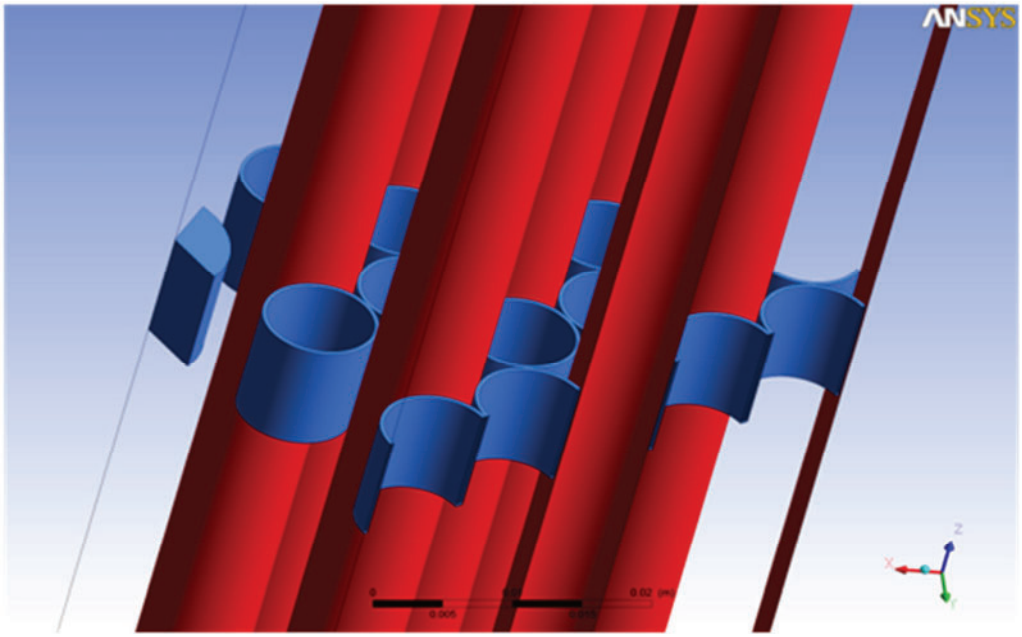

Figure 7: Thirty-seven Pin bundle 3D view

Lead Bismuth Eutectic (LBE) was considered as the working fluid for all the simulations carried out. The thermo-physical properties of LBE [8] were considered constant at the temperature T = 350 °C and are provided in Table 5.

Table 5: Thermo-physical properties of LBE at 350°C

ρ	Density	10271 kg/m^3
c_p	Specific Heat	144.81 J/kg K
μ	Dynamic Viscosity	$1.657 \cdot 10^{-3}$ Pa s
ν	Kinematic Viscosity	$1.613 \cdot 10^{-7}$ m^2/s
k	Thermal Conductivity	12.919 W/m K
α	Thermal Expansion Coefficient	$1.289 \cdot 10^{-4}$ K^{-1}

Ten steady state numerical simulations were carried out: five adopting the *SST* model and five adopting the *RSM* turbulence model. Results obtained from the simulations are reported in Table 6. In particular, Nu numbers were computed for the central sub channel and for five different inlet velocities in the range between 0.07 and 1 m/s corresponding to five different Peclet numbers.

Table 6: CFD numerical results

w [m/s]	Re [-]	Pe [-]	Nu [-] (SST)	Nu [-] (RSM)
0.07	9150	177	13.82	12.54
0.15	19600	380	14.88	13.88
0.25	32700	633	16.71	15.78
0.50	65400	1267	20.97	20.29
1.00	131000	2538	28.18	27.82

Figure 8, shows the Nu number computed from the experimental data as a function of the Pe number and a comparison with empirical correlations available in the literature. In particular, among correlations for circular rods arranged in a triangular lattice, we selected two of them, Mikityuk and Ushakov correlations (Mikityuk, 2009 [10] and Ushakov et al., 1977 [11]), with a validity range containing the *p*/*d* ratio used for the CIRCE-ICE experimental campaign.

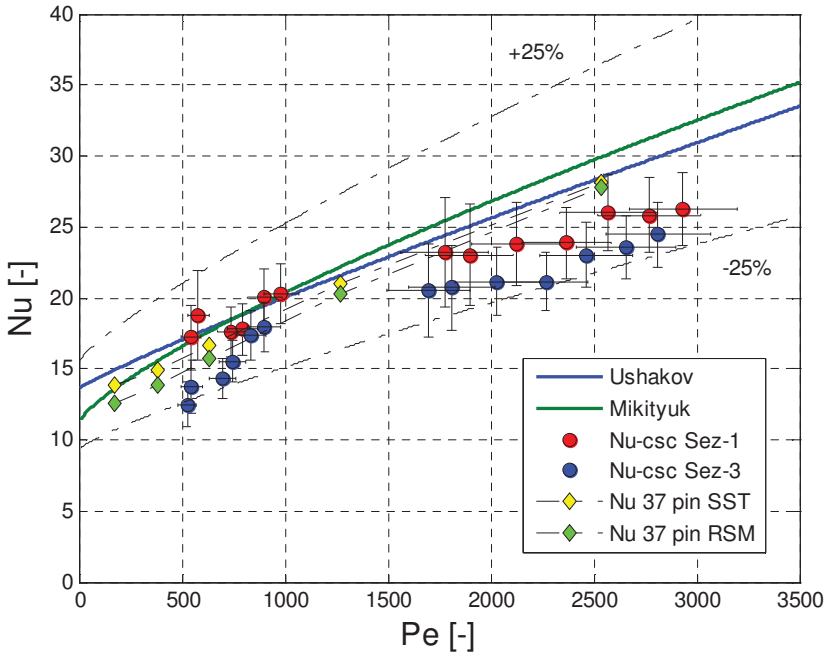

Figure 8: Nu vs. Pe number: comparison with correlations and CFD numerical results

The experimental and numerical results agree well with each other, with a general trend that slightly underestimates values obtained by correlations of Ushakov and Mikityuk. In forced circulation conditions, reducing the argon flow rate, the gas bubble flow became uneven, leading to an increase in mass flow rate dispersion of the measured data and, therefore, to an increase of the spread in temperature data in the bundle. For this reason LBE mass flow rate values lower than about 40 kg/s could not be reached in forced circulation conditions. On the other hand, the maximum LBE mass flow rate reached in natural circulation conditions without an excessive increase of the pin wall temperature is about 25 kg/s. For these reasons, experimental data cannot be obtained in the Pe range between 1000 and 1700, as shown in Figure 8. Differences between Section 1 and Section 3 are supposed to be generated by the fact that Section 1 is nearest to the spacer grid with respect to Section 3, hence, the heat transfer is most affected by the turbulence increased by the grid itself.

4. CONCLUSIONS & OUTLOOK

This work describes the experimental activity carried out at the ENEA Brasimone Research Centre dealing with the analysis of heat transfer in a 37-pin fuel rod bundle cooled with LBE under typical large pool reactor conditions.
A detailed description of the ICE Test section is presented and the instrumentation of the bundle is reported.
Then an extended characterization of the performed experiments is introduced and differences between the operation of natural and forced circulation tests are shown.
In order to obtain a standard deviation representative of the dispersion and neglecting effects due to an imperfect stationarity of acquired experimental variables, a linear regression for each gained thermocouple signal was evaluated and subtracted from the original one. In particular, linear regression was computed using the Ordinary Least Squares method (OLS). The statistical standard deviation was finally calculated using the modified data and the accuracy of instrumentation.
Moreover, the heat flux adopted in the Nusselt calculations was derived from an energy balance equation in order to take into account heat losses from the FPS wrapper to the surrounding LBE pool.
Nusselt numbers were evaluated within a Peclet range of 500-3000 assuming the hypothesis of infinite lattice.
The uncertainty of the obtained Nu is within ±16%, while the uncertainty of the Pe is within ±12%.
The Nu data were then compared with values obtained from correlations available in literature for convective heat transfer in heavy liquid metals and from CFD numerical simulations. In particular, a comparison with data obtained from Mikityuk and Ushakov correlations was presented.
Experimental and CFD data point out a linear trend in agreement with the above cited empirical correlation showing a general tendency to underestimate them; in particular, the experimental and CFD Nu values underestimated empirical data by less than 25%.
Finally, the results reported in the present work are related to the CIRCE-ICE experiments and represent the first set of experimental data concerning fuel pin bundle behaviour in a heavy liquid metal pool, both in forced and natural circulation. Future and innovative nuclear systems based on the HLM technologies (ADSs, LFRs) will be supported by these experiments in their design, safety analysis and licensing phases.

NOMENCLATURE

CFD	Computational Fluid Dynamic
CIRCE	Circulation Eutectic
ENEA	Italian National Agency for New Technologies, Energy and Sustainable Economic Development
ESNII	European Strategic Nuclear Infrastructure Initiative
EU	European Union
FC	Forced Circulation
FPS	Fuel Pin Simulator
GEN-IV	GENeration Four
Hg	Mercury
HLM	Heavy Liquid Metal
HS	Heat Source
HTC	Heat Transfer Coefficient
ICE	Integral Circulation Experiment
K	Thermal conductivity [W/(m K)]
LBE	Lead Bismuth Eutectic
LMFR	Liquid Metal Fast Reactor
LFR	Lead cooled Fast Reactor
N	Number of rods
RSM	Reynolds Stress Model
SNE-TP	Sustainable Nuclear Energy – Technology Platform
MYRRHA	Multipurpose Hybrid Research Reactor for High-tech Application
NaK	Sodium-potassium alloy
NC	Natural Circulation
OLS	Ordinary Least Squares method
Q	Thermal power [W]
SFR	Sodium Fast Reactor
SST	Shear Stress Model
TC	Thermocouple
TLOP	Total Loss Of Power
ULOF	Unprotected Loss Of Flow
ULOHS	Unprotected Loss Of Heat Sink

ACKNOWLEDGMENTS

The authors gratefully acknowledge the work done by the staff of the thermal-fluid-dynamic and facility operation laboratory of the experimental engineering technical unit of Brasimone (UTIS-TCI) for the operation of CIRCE facility, and Ing. Ranieri Marinari for its support in the CFD analysis.

REFERENCES

1. Generation IV International Forum, "Technology Roadmap Update for Generation IV Nuclear Energy Systems", January 2014.
2. Sustainable Nuclear Energy Techology Platform, "Strategic Research and Innovation Agenda" February 2013.
3. Tuček Tucek K., Carlsson J. Hartmut W., " Comparison of sodium and lead-cooled fast reactors regarding reactor physics aspects, severe safety and economical issues", Nucl. Eng. and Des. 236, pp. 1589-1598, 2006.
4. Toshinsky G.I., Komlev O. G., Tormyshev I. V., Petrochenko V.V., " Effect of Potential Energy Stored in Reactor Facility Coolant on NPP Safety and Economic Parameters", World Journal of Nuclear Science and Technology,3 pp. 59-64, 2013.
5. Sobolev V., " Thermophysical properties of lead and lead-bismuth eutectic", Journal of Nuclear Materials 362, pp. 235-247, 2007.
6. Lichten W. "Data and error analysis", Prentice Hall, 1998.
7. Moffat, R.J., "Describing the uncertainties in experimental results", Exp. Therm. Fluid Sci. 1 (1), 3–17, 1988.
8. Handbook on Lead–bismuth Eutectic Alloy and Lead Properties, Materials Compatibility, Thermalhydraulics and Technologies", 2007 edition, NEA No.6195.
9. G. Bandini, I. Di Piazza, P. Gaggini, A. Del Nevo, M. Tarantino, "CIRCE experimental set-up design and test matrix definition", ENEA UTIS-TIC Technical Report, IT-F-S-001, 28/02/2011.
10. Mikityuk K., "Heat transfer to liquid metal: review of data and correlations for tube bundles", Nuclear Engineering and Design, Vol. 239, 680–687, 2009.
11. Ushakov P.A., Zhukov A.V., Matyukhin M.M., "Heat transfer to liquid metals in regular arrays of fuel elements, High Temperature", Vol. 15, pp. 868–873, 1977; translated from Teplofizika Vysokikh Temperatur 15 (5), pp. 1027–1033, 1977.